IEEE Access
Multidisciplinary ⋮ Rapid Review ⋮ Open Access Journal

Received September 1, 2019, accepted September 14, 2019, date of current version October 4, 2019.

Digital Object Identifier 10.1109/ACCESS.2019.2942601

Generating Multiple OAM Based on a Nested Dual-Arm Spiral Antenna

YANG YANG[1,2], KAI GUO[3], FEI SHEN[2], YUBIN GONG[1], AND ZHONGYI GUO[2,3]

[1]National Key Laboratory on Vacuum Electronics, University of Electronic Science and Technology of China (UESTC), Chengdu 610054, China
[2]School of Electrical Engineering and Intelligentization, Dongguan University of Technology, Dongguan 523808, China
[3]School of Computer and Information, Hefei University of Technology, Hefei 230009, China

Corresponding authors: Yubin Gong (ybgong@uestc.edu.cn) and Zhongyi Guo (guozhongyi@hfut.edu.cn)

This work was supported in part by the National Natural Science Foundation of China (NSFC) under Grant 61531010, Grant 61775050, and Grant 11804073, and in part by the Fundamental Research Funds for the Central Universities under Grant PA2019GDZC0098, Grant JZ2018HGBZ0309, and Grant JZ2018HGTB0240.

ABSTRACT In this paper, a nested dual-arm spiral antenna (NDASA) is proposed to generate multiple orbital angular momentum (OAM) modes at the same operating frequency. The NDASA consists of the feeding network and three nested dual-arm spiral structures with different sizes. Meanwhile, a metal reflector is located between the spiral structures and the feeding network to enhance the radiation directivity, which can also reduce the impact of the radio frequency (RF) coaxial cables. Both the experimental and simulated results show OAM waves with topological charges of $l = 1$, $l = 3$ and $l = 5$ can be independently generated at $f = 3$ GHz, and their maximum gains are 6.94dBi, 6.76dBi and 5.49dBi, respectively. In addition, the OAM modes multiplexing and demultiplexing technology are investigated in simulations and experiments. The isolations between the OAM modes of $l = 1$, $l = 3$ and $l = 5$ and the other different OAM modes are greater than 13.8dB, 13.2dB and 25.1dB, respectively, which proves the potential ability of the proposed NDASA for multiplexing and demultiplexing multiple OAM modes.

INDEX TERMS Orbital angular momentum (OAM), spiral antenna, OAM multiplexing, OAM demultiplexing.

I. INTRODUCTION

In 1992, Allen *et al.* [1] discovered that orbital angular momentum (OAM) is a basic property of vortex waves, possessing a helical phase wavefront of $e^{-jl\varphi}$, where φ represents the azimuthal angle, and l is the OAM mode number called as the topological charge [2]. Since different OAM modes are orthogonal to each other, OAM can improve the spectrum efficiency and channel capacity by the method called ''mode multiplexing technique'' [3]. On one hand, some researches have been conducted on the OAM mode multiplexing and demultiplexing techniques in the optical wireless communication [4]–[6]. On the other hand, due to its potential applications, the generation and application of OAM beams have attracted many research attentions in the microwave and millimeter wave regions [7]–[21].

In 2007, OAM was firstly introduced to the radio frequency (RF) [7] and then it became a hot spot in the microwave region. To promote the practical applications of OAM, there is a strong demand for generating OAM in RF region. Different OAM states can be generated efficiently through the phased antenna array, but the complex feeding networks are necessary [8]–[13]. The spiral phase plate (SPP) structures do not require feeding network and can generate OAM beams in optical and terahertz bands through electromagnetic field diffraction [22], [23]. However, this method is restricted in the RF domain due to the intrinsic loss and reflection of SPP structures. Very recently, metasurfaces have been also proposed to generate OAM beams in the RF domain based on individually engineering the phase responses of meta-units in the azimuthal direction [24], [25]. To achieve better performance, numerous elements with different sizes and morphologies are required, making the whole design complex and bulky.

In addition, other types of antennas have been also proposed as OAM vortex waves generators to save the space and reduce the cost, such as travelling-wave-ring-slot antenna [14], [15], horn antenna [16], dielectric resonator

The associate editor coordinating the review of this manuscript and approving it for publication was Kwok L. Chung.

antenna [17], [18], conical conformal patch antenna [19], Archimedean spiral antenna [20] and helix antenna [21]. However, most of them can produce only one OAM mode [14]–[19] or different OAM modes at different frequencies [20], [21]. Since the multiple OAM states at the same frequency are necessary to improve the spectrum efficiency and channel capacity, the design of a single antenna structure for generating multiple OAM modes is very important and significant to the applications of the OAM waves.

In this paper, a multiple-mode nested dual-arm spiral antenna (NDASA) is proposed, which can generate three OAM modes simultaneously at the same operating frequency of 3GHz, independently. Three dual-arm spirals are nested with each other and are excited by different feeding networks. And the feeding networks are printed on the same substrate layer, from which the OAM multiplexing can be realized very efficiently. Meanwhile, the OAM modes multiplexing and demultiplexing technology based on the transmission system has also been investigated in simulations and experiments. The results show that the isolations among the different OAM modes are all greater than 13.2dB. Therefore, it's demonstrated that the designed NDASA has the potential ability for multiplexing and demultiplexing multiple OAM modes in efficiency.

II. GENERATION OF OAM BY PLANAR SPRIAL ANTENNA

A. THE PLANAR SINGLE-ARM SPIRAL ANTENNA

For a planar spiral antenna, whose circumference is equal to $n\lambda$, the n^{th} mode radiating from an annular ring can be excited, where λ is the free space wavelength, n is the mode number. Meanwhile, except for the first mode, these modes have ring-like intensity profiles with central nulls and the phase shifts around one circle is about $2\pi(n-1)$, which satisfies the requirement for generating OAM waves [26]. In simple words, the excitation of high-order radiation ensures the generation of vortex waves. In general, the radiations take place in the annular ring, which is called "active region", and the radius r_a satisfies the equation (1) [20]

$$r_a = \frac{C(|l|+1)}{2\pi f} \tag{1}$$

where C is the light speed, f is the operating frequency, and l is the topological charge.

The plane single-arm spiral antenna structure is presented in Fig. 1(a), and the equation of the spiral curve can be expressed as $r_1 = r_0 e^{a\varphi'} (0 < \varphi \leq 2N\pi)$, where a is the growth rate of the spiral, r_0 is the radius of the start point of the spiral, N is the number of the turn. From theoretical analysis, the E_φ component of the electric field generated by an antenna with infinite number of equiangular helical elements can be expressed as [27]:

$$E_\phi \approx \frac{\cos[\tan(\theta/2)]^l e^{(l/a)\tan^{-1}(a\cos\theta)}}{\sin\theta\sqrt{1+a^2\cos^2\theta}} \cdot e^{-j[\frac{1}{2a}\ln(1+a^2\cos^2\theta)+\tan^{-1}(a\cos\theta)]} \cdot \frac{e^{jl(\varphi+(\pi/2))-kr]}}{r} \tag{2}$$

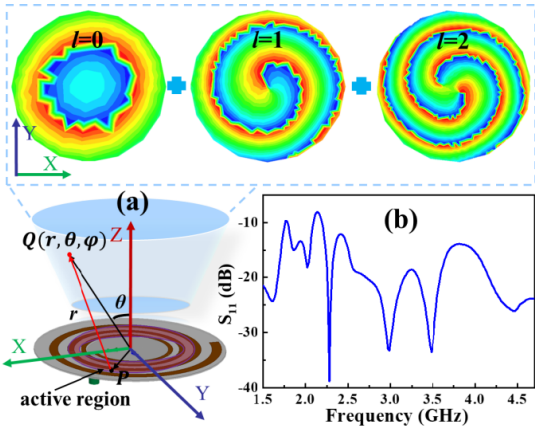

FIGURE 1. (a) Configuration and (b) the reflection coefficient of the plane single-arm spiral antenna for generating OAM.

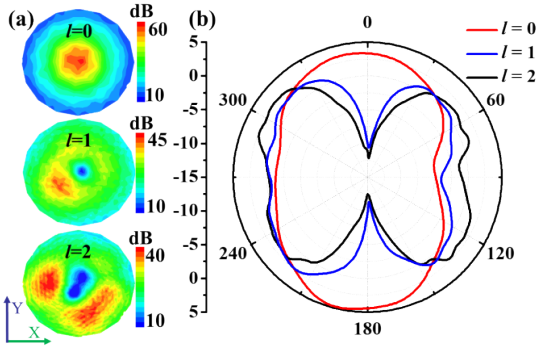

FIGURE 2. (a) The intensity distributions and (b) the 2-D far-field patterns of electric field with the topological charges of l = 0, 1 and 2, respectively.

where k is the wave number of the incident wave, φ and θ are the azimuth angle and the elevation angle of point Q respectively, r is distance between the viewing point Q and the point P in the spiral curve. Similar to the radiation mechanism of the OAM waves in [20], [27], the active region of the plane single-arm spiral antenna can radiate OAM waves with different modes of $l = 0$, 1 and 2 at the working frequency of 1.62GHz, 3GHz and 4.5GHz, respectively. In addition, the reflection coefficients in Fig. 1(b) are all below than -20dB at the corresponding frequencies of 1.62GHz, 3GHz and 4.5GHz.

The intensity distributions of electric field with the topological charges $l = 0$, 1 and 2 are shown in Fig. 2(a). The intensity of electric field with the topological charge $l = 0$ has a "hot spot" at the center while that with the topological charge $l = 1$ and 2 have a "dark spot" in the center, which fits the characteristics of the OAM waves. Meanwhile, it is clearly seen that the intensities of the electric field are asymmetric, as well as the radiation patterns, which are displayed in Fig. 2(b). The reason is that the single-arm plane spiral antenna is an asymmetric structure. To solve the problem of the asymmetric radiation, a plane dual-arm spiral antenna with symmetrical structure is proposed to radiate symmetrical OAM waves in next section.

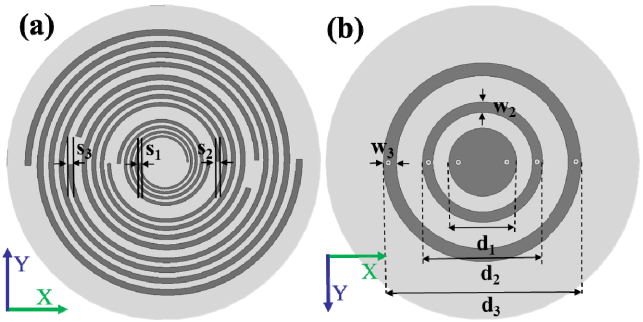

FIGURE 3. The experimental configuration of the OAM-generating system.

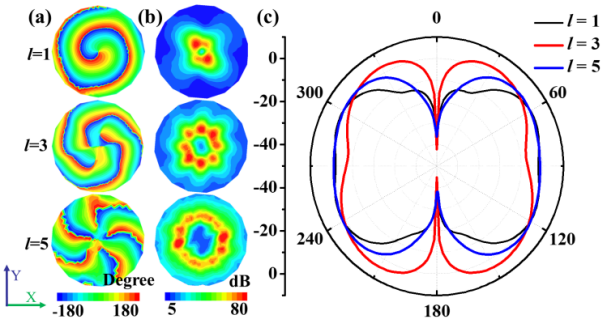

FIGURE 4. (a) The phase distributions, (b) the intensity distributions and (c) the 2D far-field radiation patterns of the plane dual-arm spiral antenna with the topological charges of l = 1, 3 and 5, respectively.

TABLE 1. The NDASA parameters.

Parameters(l=1)	a_1	r_{01}	s_1	d_1	
Values	0.05	18mm	1.36mm	26mm	
Parameters(l=3)	a_2	r_{02}	s_2	d_2	w_2
Values	0.04	43mm	2.62mm	38mm	8mm
Parameters(l=5)	a_3	r_{03}	s_3	d_3	w_3
Values	0.03	73mm	3.36mm	66mm	10mm

B. THE DESIGN OF PLANE DUAL-ARM SPIRAL ANTENNA

A NDASA is proposed to generate multiple-OAM-modes vortex waves, as shown in Fig. 3. Compared with the single-arm antenna, each arm of NDASA is composed of two spiral curves and the equations of the second curve is $r_2 = r_0 e^{a(\varphi'-\pi)} (0 < \varphi \leq 2N\pi)$. In Fig. 3(a), the microstrip spirals are printed on the top of the substrate. Fig. 3(b) presents the three metal discs with different sizes, which are printed on the bottom of the substrate. And the substrate is adopted by the 0.762mm thickness of Rogers 4350B with the relative dielectric constant of 3.48.

Based on the formula (1), in order to generate OAM waves with different modes of $l = 1$, 3 and 5 at 3GHz, the active regions with the corresponding radius of 31.8 mm, 63.7 mm and 95.5 mm are needed. Therefore, each spiral must have its corresponding size of the active region. From the theoretical analysis and simulated optimization, the dimensions of the proposed antenna can be determined. For the inner spiral, the growth rate $a_1 = 0.05$, $r_{01} = 18$mm,$s_1 = 1.36$mm and the number of the turn $N = 2$. For the middle spiral, the growth rate $a_2 = 0.04$, $r_{02} = 43$mm,$s_2 = 2.62$mm and the number of the turn $N = 1.95$. For the outer spiral, the growth rate $a_3 = 0.03$, $r_{03} = 73$mm, $s_3 = 3.36$mm and the number of the turn $N = 2$. The diameters of the three metal discs mainly for impedance matching are $d_1 = 26$mm, $d_2 = 38$mm, $d_3 = 66$mm, respectively. The widths of the middle and outer spiral are $w_2 = 8$mm and $w_3 = 10$mm, respectively. To make the values of the above parameters more clear, they are listed in Table 1.

The designed antenna structure is modeled and analyzed in the EM simulation software. The three designed spirals can generate OAM waves with different modes of l equals 1, 3 and 5, respectively. The corresponding phase distributions of electric fields are shown in Fig. 4(a), respectively. The phases of OAM waves with modes l equals 1, 3 and 5 change 2π, 6π and 10π continuously along the ring of the observing plane, respectively. Fig. 4(b) shows the intensity distributions of electric field, and there exhibit "doughnut shapes" with nulls in the center area, which demonstrates the important characteristics of vortex waves with different topological charges.

From above analysis, it is well known that the designed antenna needs multiple input ports and the phase difference of each dual-arm spirals needs be controlled accurately. In addition, Fig. 4(c) shows the 2D far-field radiation patterns of OAM waves with different topological charges of l equals 1, 3 and 5, respectively. The results demonstrate that the antenna has poor performance of far-field radiation: low gain and poor directional radiation characteristics. Therefore, the proposed antenna structure needs to be improved further.

C. THE DESIGN OF OVERALL ANTENNA STRUCTURE

To make the overall antenna structure more integrated and practical, two types of multiple input ports are needed and poor radiation performances can be improved further. The feeding network is designed to solve the problem of multiple input ports for each dual-arm spirals firstly. In addition, a metal reflector is utilized between the mircostrip spirals and the feeding network to reduce the effect of RF coaxial cable. Meanwhile, due to the 0.25λ distance between the antenna structure and the reflector, the phase differences between the radiated waves and the reflected waves by reflector are zero. Therefore, the radiated waves and reflected waves increase coherently, and then the antenna gain will be increased, which enhances the directivity of the proposed spiral antenna.

The overall antenna structure is presented in Fig. 5(a-c), in which the antenna consists of the microstrip dual-arm spirals, the feeding network and a metal reflector. The antenna is composed of three layers and six 50 Ω coaxial probes. The nested dual-arm spiral lines presented in Fig. 5 is printed on layer 1 and layer 2 is a 2mm thick aluminium plate with some holes for feeding. The feeding network on layer 3 consist of three one-to-two way power dividers and there

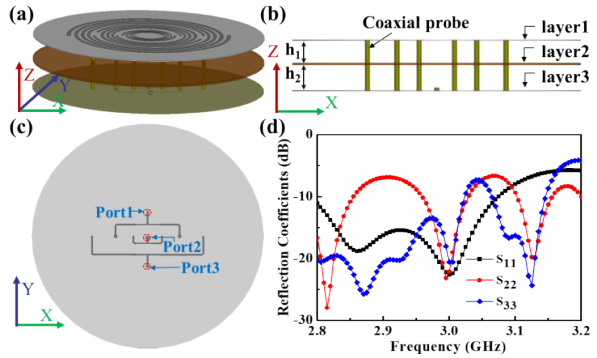

FIGURE 5. Configuration of the proposed dual-arm spiral antenna (a) 3D view, (b) side view, (c) the feeding network diagram and (d) the reflection coefficients of three feeding ports in (c).

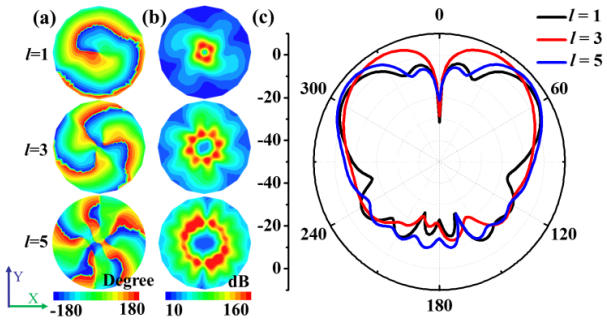

FIGURE 6. (a) The phase distributions, (b) the intensity distributions and (c) the 2D far-field radiation patterns of the proposed dual-arm spiral antenna with the topological charges of l=1, 3 and 5, respectively.

three input ports. The distances of h_1 and h_2 are 25mm and 30mm, respectively.

The proposed overall antenna structure is simulated and analyzed. The reflection coefficients of three feeding ports in Fig. 5(c) are plotted in Fig. 5(d). The antenna has multiple resonate frequencies, and the reflection coefficients of three ports can reach −15dB at the working frequency of 3GHz. In other words, the proposed antenna has the good performance of impedance matching at 3GHz. In order to obtain phase and intensity distributions of electric field at the operating frequency of 3GHz, the input ports of 1, 2 and 3 are used to excite the proposed overall antenna, respectively.

Fig. 6(a) shows the phase distributions of electric field with the topological charges of $l = 1$, 3 and 5 respectively. The corresponding intensity distributions are displayed in Fig. 6(b). All of phase and intensity distributions are in accord with classic characteristics of vortex waves with different OAM modes. In comparison to the results in Figs. 4(a-b), the feeding network and the reflector have a little effect, so the design of the overall antenna structure is reasonable for generating OAM waves. In addition, although the phase distributions have few changes, the intensities distributions are going to be more symmetrical and the hollow area of them is smaller.

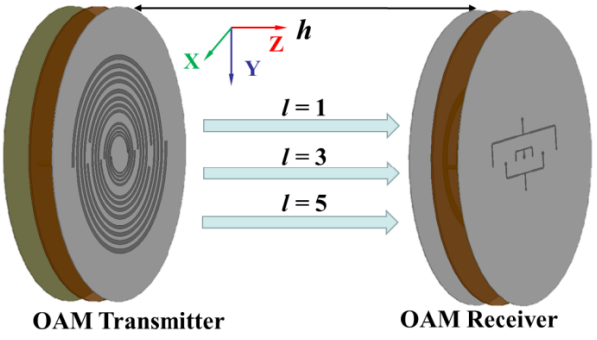

FIGURE 7. The diagram of the transmission system based on OAM transmitter and OAM receiver.

TABLE 2. Transmission characteristics between transmitting and receiving OAM modes.

dB	$l = 1$	$l = 3$	$l = 5$	Isolation
$l = 1$	-24.2	-41.9	-45.6	≥ 17.7
$l = 3$	-45.6	-26.1	-48.9	≥ 19.5
$l = 5$	-41.9	-47.8	-27.9	≥ 14

Through exciting the proposed antenna by three input ports, the 2D far-field radiation patterns are obtained. The generating OAM waves with the topological charges of $l = 1$, 3 and 5 are presented in Fig. 6(c). Compared with that in Fig. 4(c), the 2D far-field radiation patterns have higher gains and better directivity. It can be clearly seen that the corresponding gains are 6.73dBi, 6.79dBi, 5.18dBi at the OAM modes of $l = 1$, 3 and 5, respectively. In addition, the direction angle of the main lobe increases with the increasing of OAM modes l, which fits the characteristics of OAM waves.

III. OAM MULTIPLEXING AND DEMULTIPLEXING

In order to prove the orthogonality between different modes of OAM waves, a transmission system is built in the EM simulation software, shown in Fig. 7. The system consists of two identical antennas: the OAM transmitter and OAM receiver. And the two antennas paralleling in the x-y plane are placed face to face and the centers of them are aligned with a distance of h = 3λ along the z-axis. The OAM transmitter can produce vortex waves carrying the topological charges of $l = 1$, 3, and 5 by feeding three input ports, respectively, as well as the OAM receiver.

The transmission characteristics between transmitting and receiving OAM modes are concluded in Table 2. It can be seen that the transmission coefficients are higher than −27.9dB when the transmitting OAM mode is identical with the receiving OAM mode. In addition, the transmission coefficients are lower than −41.9dB when the transmitting OAM mode is non-identical with the receiving OAM mode. When transmitting OAM mode $l = 1$, isolation between receiving

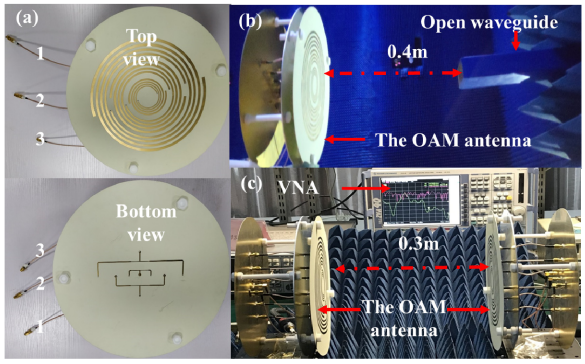

FIGURE 8. (a) Prototype of the fabricated overall antenna structure, (b) the near-field test scenario, and (c) S parameters test scenario.

OAM modes $l = 1$ and $l \neq 1$ is higher than 17.7dB. Similarly, when transmitting OAM mode $l = 3$ and 5, the isolation is higher than 19.5dB and 14dB, respectively. The results demonstrate the orthogonality between different modes of OAM waves. Hence, the method has a potential ability to demultiplex and detect multiple OAM modes.

IV. FABRICATION AND MEASUREMENT OF THE VERALL ANTENNA STRUCTUER

To verify the simulated results of the overall antenna structure, a prototypes was fabricated and measured accordingly. Prototype of the fabricated overall antenna structure, the near-field test scenario and S parameters test scenario are shown in Figs. 8(a-c), respectively. In Fig 8(a), the coaxial lines 1, 2 and 3 connect port 1, 2 and 3 which are shown in Fig. 5(c), respectively. A vector network analyzer (VNA, Rohde & Schwarz, ZVA 40) is used to measure the reflection coefficients of the three ports and transmission coefficients between six ports while two loads of 50Ω serve as the impedance matching. In addition, for measuring the near-field distributions, an open waveguide is used as the detecting antenna to receive the radiated field. The sampling plane of the detecting probe paralleling in the x–y plane is 0.4m away from OAM antenna along the z-axis. The size of it is 2.52m × 1.68m, and the number of the sampling points is 59 × 40.

The experimental reflection coefficients and transmission coefficients of the six ports are presented in Figs. 9(a-b), respectively. Although there is a little difference caused by processing and assembling errors between experimental results and simulated ones, it does not influence its performance. It is clearly seen that the values of all the lines in Fig. 9(a) are below than −10dB and each is almost the same to another at 2.96GHz in orange circle. Therefore, the reflections have less influence on the transmission coefficients around 2.96GHz and the transmission coefficients are presented in Fig. 9(b). The measured transmission coefficients have included the loss of the measuring instruments, so it is lower than simulated ones. Fortunately, the transmissions between different OAM modes is much more different at 2.98GHz in green circle and the isolations between the OAM

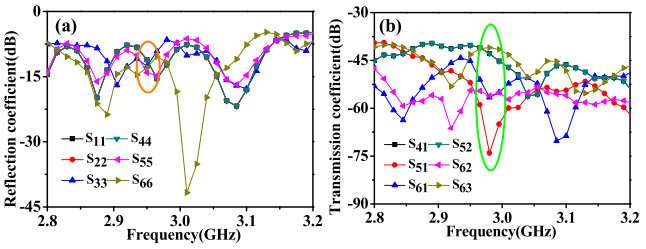

FIGURE 9. (a) The reflection coefficients and (b) the transmission coefficients of the six ports in the overall antenna structure.

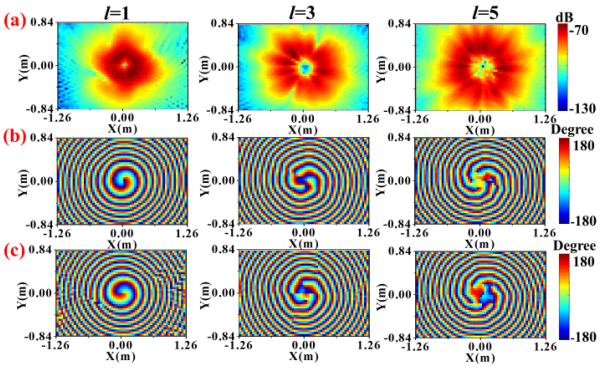

FIGURE 10. The experimental (a) intensities of the total near-field and the phase distributions of (b) x-component and (c) y-component at 3GHz with the modes of l = 1, l = 3 and l = 5.

modes of $l = 1$, $l = 3$ and $l = 5$ and the other different OAM modes are greater than 13.8dB, 13.2dB and 25.1dB, respectively, which demonstrates the ability of the proposed method to demultiplex and detect multiple OAM modes. Moreover, the frequency of 2.98GHz is just close to that frequency in orange circle of Fig. 9(a).

The experimental intensities of the total near-field and the phase distributions of x-component and y-component at 3GHz with the modes of $l = 1$, 3 and 5 are presented in Figs. 10(a-c), respectively. The intensities distributions satisfy the "donut shape" and the phases distributions satisfy the "spiral shape", which shows their good performances. In addition, the null of the intensities, the phase shifts and the directions of phase rotation are also consistent with simulation ones. However, there are a few haphazard distributions in center area. The reason is just that these fields are too small to be detected by measuring instruments.

In order to generate the far-field patterns at 3GHz, following Huygens principle, the measured data in the near field can be easily transformed into the far field by the inverse Fourier transform [28]. The experimental 3D far-field intensities and phase patterns at 3GHz with the different OAM modes of $l = 1$, 3 and 5 are displayed in Figs. 11(a-b), respectively. The intensities and phase patterns distributions are more in line with the characteristics of corresponding vortex waves, demonstrating their good radiation performance. The maximum gain of $l = 1$, 3 and 5 are 6.94dBi, 6.76dBi and 5.49dBi, respectively, which agree with the simulated ones.

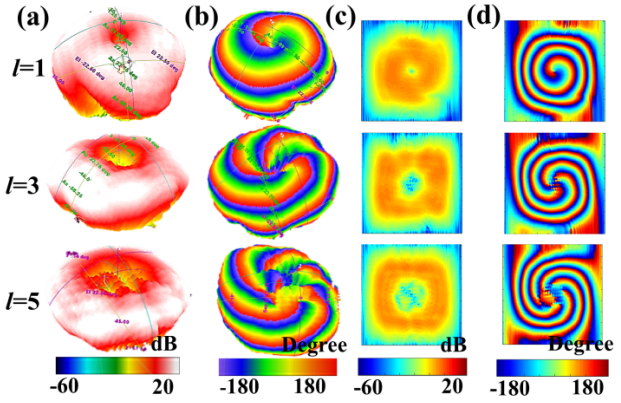

FIGURE 11. The experimental far-field 3D results of (a) intensities and (b) phase patterns, and 2D results of (c) intensities and (d) phase patterns, at 3GHz with the different OAM modes of l = 1, l = 3 and l = 5, respectively.

TABLE 3. Performance comparisons with reported OAM antennas.

*Ref	Antenna Structure	Size	f_0 (GHz)	*EFN	OAM Modes	Gain (dBi)
[15]	Cavity + slot + Horn	$\Phi 4.12\lambda_0$	10	YES	2,3,4	3.71
[16]	Horn antenna	$\Phi 1.3\lambda_0\times$ 91mm	9.2	YES	±1	N.A
[18]	hemispherical dielectric resonator	$\Phi 2.48\lambda_0$	5.8	NO	±1	5.8
[19]	Conical conformal MP	$\Phi 3.625\lambda_0$ ×28mm	2.4	YES	±1 ±2	6.6 N.A
[20]	MP + cavity	Φ200mm ×80mm	3 4 4.8	YES	±1 ±2 ±3	6.7~10
[21]	Cavity + three-dimensional helical	Φ100mm ×50mm	0.76 1.55 2.45	YES	0 1 2	<4.55
Our work	Spiral antenna	$\Phi 3\lambda_0\times$ 57mm	3	NO	1 3 5	6.94 6.76 5.49

*MP: microstrip-patch *EFN: extra feeding network *N.A: not available.

For further demonstrating the quality of the generated OAM waves, by the same method mentioned above, the experimental 2D far-field intensities and phase distributions at 3GHz with the different co-polarized OAM modes of $l = 1$, 3 and 5 are displayed in Figs. 11(c-d), respectively. It can be seen that both the intensity and phase distributions are smooth and rounded, which agrees with the characteristics of OAM very well, and also demonstrates the good performance of the proposed antenna.

In order to prove the advantages of the proposed antenna, we have also listed the performances' comparisons with other similar structures in Table 3. Due to faster growth rate, there is lower loss on the metal spiral, so it has higher gain when comparing with the structures in [15], [21]. Due to the nested structure, the proposed antenna is relatively smaller than the structures in [15], [16], [19], [20]. In addition, although the whole mentioned structures have the ability to produce multiple OAM waves, only the proposed antenna can produce multiple OAM waves at the same frequency, simultaneously. Once the structures of the other antenna are determined, the generated OAM mode $|l|$ is determined. Except the structure in [18] and our designed antenna, these structures all need an extra feeding network. Last but not the least, our proposed antenna can generate OAM waves with the higher order of $l = 5$.

V. CONCLUSION

A nested dual-arm spiral antenna is designed to generate multiple OAM beams at the same working frequency of 3GHz. Through the excitation of the feeding network, OAM waves are generated by the plane dual-arm spiral structure. The metal reflector between the mircostrip spiral and the feeding network is used to enhance the directivity and reduce the impact of the RF coaxial cables. The proposed antenna can produce vortex waves with OAM modes of $l = 1$, 3 and 5 at an operating frequency of 3GHz, simultaneously. The designed antenna is simulated, fabricated and measured. The maximum gains of $l = 1$, 3 and 5 are 6.94dBi, 6.76dBi and 5.49dBi, respectively. In addition, the OAM modes multiplexing and demultiplexing technology is investigated in simulations and experiments, from which it can be seen that the isolations between the OAM modes of $l = 1$, $l = 3$ and $l = 5$ and the other different OAM modes are greater than 13.8dB, 13.2dB and 25.1dB, respectively. Therefore, the potential ability of designed NDASA for multiplexing and demultiplexing multiple OAM modes is proven.

REFERENCES

[1] L. Allen, M. Beijersbergen, R. Spreeuw, and J. Woerdman, "Orbital angular momentum of light and the transformation of Laguerre–Gaussian laser modes," *Phys. Rev. A, Gen. Phys.*, vol. 45, no. 11, p. 8185, 1992.
[2] Z. Guo, L. Zhu, K. Guo, F. Shen, and Z. Yin, "High-order dielectric metasurfaces for high-efficiency polarization beam splitters and optical vortex generators," *Nanoscale Res. Lett.*, vol. 12, no. 1, p. 512, 2017.
[3] J. Sjoholm and K. Palmer, "Angular momentum of electromagnetic radiation," M.S. thesis, Uppsala School Eng. Dept. Astronomy Space Phys., Uppsala Univ., Uppsala, Sweden, 2007.
[4] C. Kai, P. Huang, F. Shen, H. Zhou, and Z. Guo, "Orbital angular momentum shift keying based optical communication system," *IEEE Photon. J.*, vol. 9, no. 2, Apr. 2017, Art. no. 7902510.
[5] C. Kai, Z. Feng, M. I. Dedo, P. Huang, K. Guo, F. Shen, J. Gao, and Z. Guo, "The performances of different OAM encoding systems," *Opt. Commun.*, vol. 430, pp. 151–157, Jan. 2019.
[6] Z. Guo, Z. Wang, M. I. Dedo, and K. Guo, "The orbital angular momentum encoding system with radial indices of Laguerre–Gaussian beam," *IEEE Photon. J.*, vol. 10, no. 5, Oct. 2018, Art. no. 7906511.
[7] B. Thidé, H. Then, J. Sjöholm, K. Palmer, J. Bergman, T. D. Carozzi, Y. N. Istomin, N. H. Ibragimov, and R. Khamitova, "Utilization of photon orbital angular momentum in the low-frequency radio domain," *Phys. Rev. Lett.*, vol. 99, no. 8, Aug. 2007, Art. no. 087701.
[8] Y.-M. Zhang and J.-L. Li, "An orbital angular momentum-based array for in-band full-duplex communications," *IEEE Antennas Wireless Propag. Lett.*, vol. 18, no. 3, pp. 417–421, Mar. 2019.
[9] X.-D. Bai, X.-L. Liang, Y.-T. Sun, P.-C. Hu, Y. Yao, K. Wang, J.-P. Geng, and R.-H. Jin, "Experimental array for generating dual circularly-polarized dual-mode OAM radio beams," *Sci. Rep.*, vol. 7, Jan. 2017, Art. no. 040099.
[10] H. Li, L. Kang, F. Wei, Y.-M. Cai, and Y.-Z. Yin, "A low-profile dual-polarized microstrip antenna array for dual-mode OAM applications," *IEEE Antennas Wireless Propag. Lett.*, vol. 16, pp. 3022–3025, 2017.

[11] T. Yang, D. Yang, B. Wang, and J. Hu, "Experimentally validated, wideband, compact, OAM antennas based on circular vivaldi antenna array," *Prog. Electromagn. Res. C*, vol. 80, pp. 211–219, Jan. 2018.
[12] Y.-Y. Wang, Y.-X. Du, L. Qin, and B.-S. Li, "An electronically mode reconfigurable orbital angular momentum array antenna," *IEEE Access*, vol. 6, pp. 64603–64610, 2018.
[13] L. Li and X. Zhou, "Mechanically reconfigurable single-arm spiral antenna array for generation of broadband circularly polarized orbital angular momentum vortex waves," *Sci. Rep.*, vol. 8, no. 1, p. 5128, Mar. 2018.
[14] W. Zhang, S. Zheng, X. Hui, Y. Chen, X. Jin, H. Chi, and X. Zhang, "Four-OAM-mode antenna with traveling-wave ring-slot structure," *IEEE Antennas Wireless Propag. Lett.*, vol. 16, pp. 194–197, 2016.
[15] Z. Zhang, S. Zheng, X. Jin, H. Chi, and X. Zhang, "Generation of plane spiral OAM waves using traveling-wave circular slot antenna," *IEEE Antennas Wireless Propag. Lett.*, vol. 16, pp. 8–11, 2016.
[16] M. Huang, X. Zong, and Z. P. Nie, "Horn antenna generating electromagnetic field with orbital angular momentum," *Prog. Electromagn. Res. M*, vol. 60, pp. 57–65, Oct. 2017.
[17] J. Liang and S. Zhang, "Orbital angular momentum (OAM) generation by cylinder dielectric resonator antenna for future wireless communications," *IEEE Access*, vol. 4, pp. 9570–9574, 2016.
[18] J. Ren and K. W. Leung, "Generation of microwave orbital angular momentum states using hemispherical dielectric resonator antenna," *Appl. Phys. Lett.*, vol. 112, no. 13, Mar. 2018, Art. no. 131103.
[19] F. Shen, J. Mu, K. Guo, and Z. Guo, "Generating circularly polarized vortex electromagnetic waves by the conical conformal patch antenna," *IEEE Trans. Antennas Propag.*, vol. 67, no. 9, pp. 5763–5771, Sep. 2019.
[20] L. Wang, H. Chen, K. Guo, F. Shen, and Z. Guo, "An inner- and outer-fed dual-arm archimedean spiral antenna for generating multiple orbital angular momentum modes," *Electronics*, vol. 8, no. 2, p. 251, 2019.
[21] F. Shen, J. Mu, K. Guo, S. Wang, and Z. Guo, "Generation of continuously variable-mode vortex electromagnetic waves with three-dimensional helical antenna," *IEEE Antennas Wireless Propag. Lett.*, vol. 18, no. 6, pp. 1091–1095, Jun. 2019.
[22] Z. Guo, Z. Li, J. Zhang, K. Guo, F. Shen, Q. Zhou, and H. Zhou, "Review of the functions of Archimedes' spiral metallic nanostructures," *Nanomaterials*, vol. 7, no. 11, p. 405, 2017.
[23] L. Zhu, X. Wei, J. Wang, Z. Zhang, Z. Li, H. Zhang, S. Li, K. Wang, and J. Liu, "Experimental demonstration of basic functionalities for 0.1-THz orbital angular momentum (OAM) communications," in *Proc. OFC*, Mar. 2014, pp. 1–3.
[24] K. Sueda, G. Miyaji, N. Miyanaga, and M. Nakatsuka, "Laguerre–Gaussian beam generated with a multilevel spiral phase plate for high intensity laser pulses," *Opt. Express*, vol. 12, no. 15, pp. 3548–3553, 2004.
[25] S. Yu, L. Li, G. Shi, C. Zhu, and Y. Shi, "Generating multiple orbital angular momentum vortex beams using a metasurface in radio frequency domain," *Appl. Phys. Lett.*, vol. 108, no. 24, May 2016, Art. no. 241901.
[26] R. C. Johnson and H. Jasik, "Frequency-independent antennas," in *Antenna Engineering Handbook*, 3rd ed. New York, NY, USA: McGraw-Hill, 1993, pp. 1–10.
[27] B. Cheo, V. Rumsey, and W. Welch, "A solution to the frequency-independent antenna problem," *IRE Trans. Antennas Propag.*, vol. 9, no. 6, pp. 527–534, Nov. 1961.
[28] W. L. Stutzman and G. A. Thiele, *Antenna Theory and Design*, 3rd ed. New York, NY, USA: Wiley, 2012.